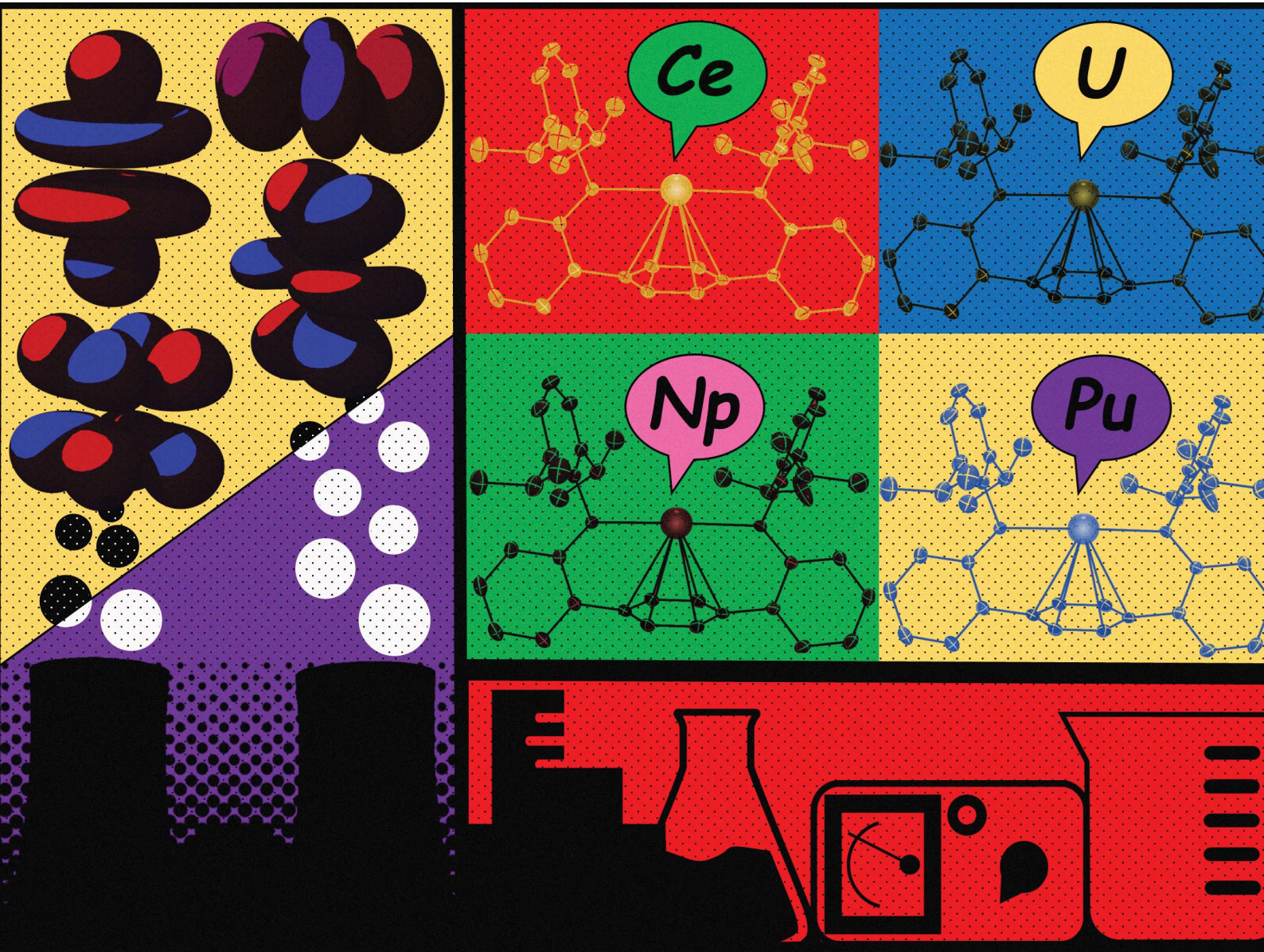


Chemical Science

rsc.li/chemical-science



ISSN 2041-6539

Cite this: *Chem. Sci.*, 2023, **14**, 7438

All publication charges for this article have been paid for by the Royal Society of Chemistry

Received 29th April 2023
Accepted 10th June 2023

DOI: 10.1039/d3sc02194g
rsc.li/chemical-science

Synthesis and comparison of iso-structural f-block metal complexes (Ce, U, Np, Pu) featuring η^6 -arene interactions†

Jesse Murillo,^{ab} Conrad A. P. Goodwin,^b Lauren Stevens,^{bc} Skye Fortier,^b Andrew J. Gaunt^b* and Brian L. Scott^c

Reaction of the terphenyl bis(anilide) ligand $[(K(DME)_2)_2 L^{Ar}]$ ($L^{Ar} = \{C_6H_4[(2,6-iPr^2C_6H_3)NC_6H_4]_2\}^{2-}$) with trivalent chloride "MCl₃" salts ($M = Ce, U, Np$) yields two distinct products; neutral $L^{Ar}M(Cl)(THF)$ (**1^M**) ($M = Np, Ce$), and the "-ate" complexes $[(K(DME)_2)[(L^{Ar})Np(Cl)_2]]^{2-}$ (**2^{Np}**) or $[(L^{Ar}M(Cl)_2(\mu-K(X)_2))]_{\infty}$ (**2^{Ce, U}**) ($M = Ce, U$ ($X = DME$ or Et_2O)) (**2^M**). Alternatively, analogous reactions with the iodide $[M I_3(THF)_4]$ salts provide access to the neutral compounds $L^{Ar}M(I)(THF)$ (**3^M**) ($M = Ce, U, Np, Pu$). All complexes exhibit close arene contacts suggestive of η^6 -interactions with the central arene ring of the terphenyl backbone, with **3^M** comprising the first structurally characterized Pu η^6 -arene moiety. Notably, the metal–arene bond metrics diverge from the predicted trends of metal–carbon interactions based on ionic radii, with the uranium complexes exhibiting the shortest M–C_{centroid} distance in all cases. Overall, the data presents a systematic study of f-element M– η^6 -arene complexes across the early actinides U, Np, Pu, and comparison to cerium congeners.

Introduction

Moving towards a more detailed understanding of chemical behaviour and bonding trends within the 5f-block elements has been of keen interest since the proposal of the actinide (An) concept by Seaborg in the later part of the 1930's.¹ Once thought to predominantly engage in metal–ligand bonding chiefly electrostatic in nature, decades of concerted advances in the syntheses and characterization of actinide-containing molecular complexes have demonstrated the ability of actinide metal ions to form covalent bonds. These interactions are generally intermediate between that of transition metals (highly directional based on metal–ligand orbital overlap), and lanthanides (non-directional).^{2–10} In several cases, actinide–ligand interactions are not purely electrostatic in nature and are engendered by the availability of 6d and 5f orbitals to participate in bonding, especially for the early actinide members (An = U, Np, Pu).^{10–23}

Of note, f-block metal complexes which contain metal–arene interactions have proven to be highly valuable for understanding bonding and the role of valence orbitals for

lanthanides and actinides.^{24–32} Among this class of molecules, those which feature neutral arene coordinating motifs are of particular interest as these may exhibit covalent participation of the metal in the form of $\pi/\delta/\varphi$ type interactions.^{31,33–37} Such complexes have potential to provide new key insight into f-block bonding modes as has been the case in other areas of the periodic table; for example, the seminal discovery of bis(benzene)chromium, $Cr(\eta^6-C_6H_6)_2$, by E. O. Fischer, which revolutionized the understanding of transition metal chemistry.³⁸

A challenge to overcome in establishing a suite of analogous metal–arene molecules across the f-block is the "hard" Lewis acidic character of the f-block metal ions that causes interactions with "soft" arene donor substituents to be difficult to form and have often required the use of hard donor atom substituents to act as an "anchor-point" and facilitate binding of the arene to the metal.^{35,36,39–50} A handful of examples exist which do coordinate neutral arene species by coordinating strongly electron withdrawing groups to the actinide.^{51–57} Indeed, despite their challenging synthetic nature, several milestone works have successfully accessed and isolated actinide–arene complexes. Notably, the work of Meyer and co-workers to form the tris(aryloxide) uranium(III) complex, $[(^{Ad,Me}ArO)_3mes]U$, has illustrated the utility of the tethered arene strategy and led to the formation of low-valent (2+) uranium complexes, which show remarkable reactivity and are stabilized by unique actinide–arene bonding motifs.^{35,39–41,58,59} Later work by Arnold and co-workers extended this strategy to a transuranium element, neptunium, by the formation of several complexes featuring Np-

^aDepartment of Chemistry and Biochemistry, University of Texas at El Paso, El Paso, Texas 79968, USA. E-mail: asfortier@utep.edu

^bChemistry Division, Los Alamos National Laboratory, Los Alamos, New Mexico 87545, USA. E-mail: gaunt@lanl.gov

^cMaterials Physics and Applications Division, Los Alamos National Laboratory, Los Alamos, New Mexico 87545, USA

† Electronic supplementary information (ESI) available. CCDC 2238465–2238473. For ESI and crystallographic data in CIF or other electronic format see DOI: <https://doi.org/10.1039/d3sc02194g>



η^6 -arene interactions, facilitated by the *trans*-calix[2]benzene[2]pyrrole ligand platform.²¹

We recently employed a terphenyl bis(anilide) ligand system $[L^{Ar}]$ ($L^{Ar} = \{C_6H_4[(2,6-iPr^2C_6H_3)NC_6H_4_2]\}^{2-}$),⁴⁶ which features aromatic substituents in the ligand backbone that, upon complexation with Ln/An metal ions, binds in a $\kappa^2:\eta^6$ -fashion. We found this ligand platform to have remarkable versatility.^{46,47,60} Given that the $[L^{Ar}]$ ligand platform has been demonstrated to coordinate both Dy and U, in addition to the architectural enforcement of a metal- η^6 -arene interaction upon complexation, we felt this ligand system would serve as an excellent foundation for forming iso-structural complexes of f-block elements, including transuranium species, allowing us to gain insight into metal-arene bonding interactions and elucidate periodic trends. Based upon ionic radii alone, we expected to observe a metal-arene distance trend $U > Ce \sim Np > Pu$ if a purely electrostatic bonding model adequately described the bonding. Conversely, if deviations from that trend were observed, then that may be suggestive of metal-ligand covalent interactions more pronounced in some of the f-metal complexes than others.

Results and discussion

The reaction of the dipotassium salt of the ligand, $[(K(DME)_2)_2L^{Ar}]$, with 1 equiv. of "MCl₃" at room temperature in THF formed a deep brown/red turbid solution ($M = U, Np$) or a bright yellow/orange turbid solution ($M = Ce$) (Scheme 1). The U and Np trivalent chloride metal precursors were formed by the *in situ* reduction of tetravalent UCl₄ and NpCl₄(DME)₂ in THF using 1.1 equiv. of potassium graphite (KC₈), forming presumed MCl₃(THF)_n adducts, while the Ce source was commercially purchased CeCl₃. Drying the reaction mixture and extracting with Et₂O, presents a dark red solution ($M = Np, U$) or a vivid yellow solution ($M = Ce$), which upon workup and storage at -35 °C provides crystals suitable for single-crystal X-ray diffraction (SC-XRD) and were identified as $L^{Ar}M(Cl)(THF)$ (1^M) ($M = Ce, Np$) (Fig. 1 and S1†) isolated in relatively low yields

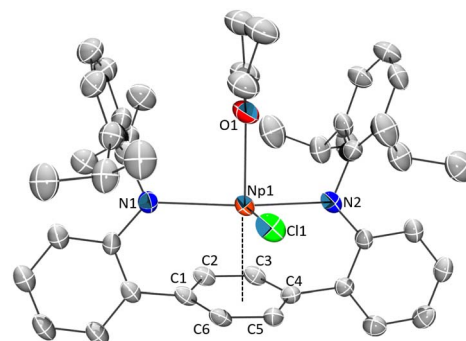
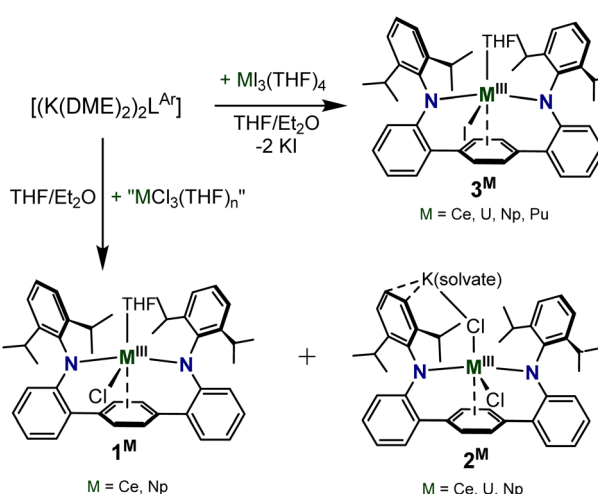


Fig. 1 ORTEP of the solid-state molecular structure of 1^{Np} . Hydrogen atoms and co-crystallized Et₂O molecule are removed for clarity. Ellipsoids are shown at the 30% probability level. Shown for connectivity purposes only.

(20% for 1^{Np} and 11% for 1^{Ce}). For $M = U$, the Et₂O extract failed to give the analogous 1^U complex, but instead formed the contact polymer $[L^{Ar}M(Cl)_2\{\mu-K(Et_2O)_2\}]_\infty$ (2^U), isolated in 28% yield. Attempts to generate and isolate the Pu congener, 1^{Pu} , using *in situ* generated PuCl₃(THF)_x *via* reduction of PuCl₄(-DME)₂, to enable a systematic U/Np/Pu comparison, were unsuccessful and yielded intractable products.

The Et₂O insoluble products from the reactions are highly soluble in DME (DME = 1,2-dimethoxyethane) or THF to give dark red/brown solutions ($M = Np, U$), or a dark orange solution ($M = Ce$). These solutions, after workup and storage at -35 °C for several days, give X-ray quality single-crystals identified as the "ate" complex $[K(DME)_2(L^{Ar})Np(Cl)_2]$ (2^{Np}) or the contact polymer $[L^{Ar}M(Cl)_2\{\mu-K(x)_2\}]_\infty$ (2^{Ce}) ($X = DME$ or Et₂O) (Scheme 1) in 20% and 10% yields respectively. In the case of the uranium reaction, the THF extract produced intractable products, although on one attempt we were able to isolate the 1-D polymeric complex $[L^{Ar}U(Cl)_2(THF)\{\mu-K(THF)_4\}]_\infty$, where the uranium metal ions are bridged by Cl-K-Cl contacts (Fig. S2†). In the case of 2^{Np} , the complex exists as a discrete molecular species in the solid-state, where the potassium ion is contacting the apical chloride and is coordinated by two DME molecules, while one non-coordinated DME molecule is located in the lattice (Fig. 2). In complexes 2^{Ce} and 2^U the potassium ions are coordinated by a mix of DME and Et₂O solvates that act as bridging moieties, forming 1-D polymeric species (see Fig. S3 and S4† for extended structures). For 2^{Ce} and 2^U , disordered hexane molecules fill the void space within the crystal lattice. Although the solid-state arrangement differs, the anionic component of the 2^M series is homologous and are shown in Fig. 2.

The ¹H NMR spectra of 1^M and 2^M span a large range of chemical shifts (characteristic of the metal ion electronic configurations - Ce³⁺(4f¹), U³⁺(5f³), Np³⁺(5f⁴)), showing proton resonances within the range from -30.65 to +42.22 ppm for the six complexes (Fig. S8-S12†). In accordance with low-symmetry molecular environments in solution, the complicated spectra are typical of previously reported complexes of $[L^{Ar}]$, some of which display dozens of unique resonances in their ¹H NMR spectra.^{46,47,60} For all complexes, except for 2^U , resonances for



Scheme 1 Syntheses of 1^M , 2^M , and 3^M .



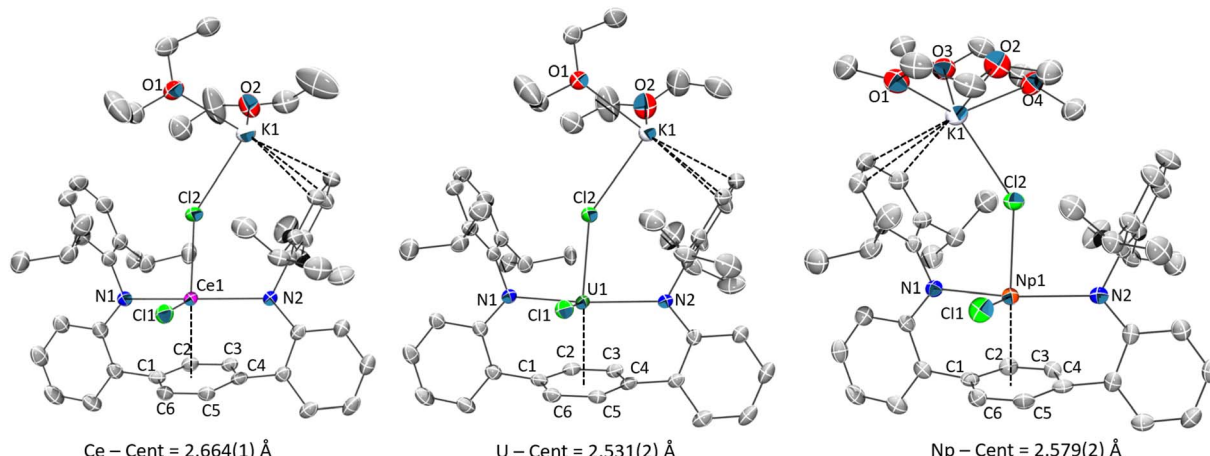


Fig. 2 ORTEP of the solid-state molecule structures of $2^{Ce}\cdot 2\text{Hex}$ (left), $2^U\cdot 2\text{Hex}$ (centre), and $2^{Np}\cdot \text{DME}$ (right). Hydrogen atoms and co-crystallized solvents are removed for clarity. Ellipsoids are shown at the 50% probability level.

the protonated ligand, $\text{H}_2\text{L}^{\text{Ar}}$, can be seen in the ^1H NMR spectra. The quantity of $\text{H}_2\text{L}^{\text{Ar}}$ varies among the measured spectra but is consistently observed by ^1H NMR spectroscopy. The majority of ^1H NMR spectra were collected on isolated crystalline material of the complexes, which suggests that the formation of $\text{H}_2\text{L}^{\text{Ar}}$ may be taking place in solution. However, the presence of small amounts of $\text{H}_2\text{L}^{\text{Ar}}$ as a crystalline by-product cannot be definitively discounted.

Single-crystal X-ray structures 1^M and 2^M show a common coordination geometry, with all complexes displaying a pseudo four-coordinate, see-saw type geometry around the metal centre (Fig. 1, 2 and S1†). The $[\text{L}^{\text{Ar}}]$ ligand binds in a κ^2 -mode *via* the anilide N-donor atoms, which are approximately in the *trans* configuration (Tables 1, S4†). With respect to key structural parameters, only minor disparities between the neutral 1^M and “-ate” 2^M complexes are observed, although rigorous metrical comparisons of 1^{Np} are not possible due to the poor quality of X-ray data for that complex. A significant shortening of the M-Cl bond in the neutral complex 1^{Ce} is seen as compared to 2^{Ce} , when taking the average M-Cl bonding value for 2^{Ce} and the replacement of the apical Cl^- anion with a neutral THF molecule in 1^M vs. 2^M (Tables 1 and S4†). Given the broad similarities in the metal-ligand interactions, and the superior quality SC-XRD data for the 2^M series, we will discuss in detail only 2^M structures in the following section.

Selected bond metrics for the 2^M series are shown in Table 1. It is important to note here that although the anionic core of these structures is similar, they differ in their extended structures with 2^{Ce} and 2^U being polymeric while 2^{Np} is a discrete

molecule. Additionally, the potassium coordinated, and non-coordinated lattice solvents differ in identity and relative amounts across the series. While these differences likely influence bonding metrics, we point out that trends found in the 2^M series are mimicked in the 1^M and 3^M (*vide infra*) complexes. With these distinctions in mind, we next discuss in more detail bonding features discovered in the 2^M series.

The M-N bond distances for all complexes are within the expected range for amide-M(III) bonds of their type, though they tend towards the longer end of the reported ranges.^{21,47,61-64} Additionally, there are no clear statistically meaningful differences in the M-N metrics as a function of f-metal identity. On the other hand, subtle yet significant distinctions can be observed with respect to the M-C_{arene} interactions among the 2^M compounds. Curiously, these disparities do not seem to trend with a purely electrostatic model based on metal ionic radius.

The metal-arene centroid distance, M-C_{cent}, among the series is shortest in 2^U at 2.530 (1) Å and longest in 2^{Ce} at 2.664 (1) Å ($\Delta = 0.134$ Å), despite the reported six-coordinate ionic radius of Ce^{3+} being smaller than U^{3+} ($\Delta = 0.015$ Å).⁶⁵ Compound 2^{Np} has an intermediate value at 2.579 (2) Å which is 0.085 Å shorter than in 2^{Ce} and 0.049 Å longer than in 2^U . For context, Np^{3+} has an ionic radii essentially identical to Ce^{3+} (both 1.01 Å) and therefore equally smaller than U^{3+} ($\Delta = 0.015$ Å).⁶⁵ These differences are noteworthy because, if following an ionic bonding model, the 2^U complex should possess slightly longer M-C_{cent} contacts than in the 2^{Ce} and 2^{Np} complexes (not accounting for steric congestion changes and lattice packing

Table 1 Selected bond metrics for the 2^M series

Complex	M-N bond distances (Å) (N ₁ /N ₂)	M-cent distance (Å)	M-C _{arene} range (Å)	M-Cl distance (Å) (Cl ₁ /Cl ₂)	Cl ₂ -M-Cl ₁ bond angle (°)	N-M-N bond angle (°)	Metal ionic radius (Å)
$2^{Ce}\cdot 2\text{Hex}$	2.470 (2)/2.525 (2)	2.664 (1)	2.936 (2)-3.092 (2) avg. 3.01	2.669 (1)/2.687 (1)	101.90 (3)	156.36 (7)	1.01
$2^U\cdot 2\text{Hex}$	2.452 (3)/2.509 (3)	2.530 (1)	2.834 (4)-2.959 (4) avg. 2.89	2.670 (1)/2.689 (1)	101.39 (4)	157.8 (1)	1.025
$2^{Np}\cdot \text{DME}$	2.494 (4)/2.483 (4)	2.579 (2)	2.911 (5)-2.966 (5) avg. 2.93	2.627 (1)/2.674 (1)	101.09 (4)	156.3 (1)	1.01



effects). Similarly, the range of the metal–arene carbon bonds in 2^U are shorter than in the Ce and Np analogues, a fact reflected in the average M–C_{arene} bond distances.

In general, the internal C–C bonds of the η^6 -coordinated ring display alternating short-long bond distances for all 2^M (Table S5†) along with subtle out-of-plane distortions across the ipso-substituents of the central ring (C1–C_{cent}–C4; 7.8, 8.7, and 7.6° for M = Ce, Np, U, respectively) (Fig. S36†). These features are consistent with previous similar observations in some other metal–arene complexes.^{66–68}

When switching the metal precursor source to the well-defined trivalent iodide starting material $MI_3(THF)_4$ (M = U, Np, Pu)^{69,70} or commercially sourced CeI_3 , reactions with $[(K(DME)_2)_2L^{Ar}]$ in THF consistently yield the monomeric neutral $L^{Ar}M(I)(THF)$ (3^M) complex. Gratifyingly, the 3^M series facilitated inclusion of Pu, as 3^{Pu} (Fig. 3), which to the best of our knowledge is the first reported plutonium complex containing an η^6 -coordinated arene ring. These complexes are neutral in character and lack the potassium ion found in 2^M . The lack of the “-ate” complex formation in the case of the $MI_3(THF)_4$ reactions we attribute to the larger ionic radius of the I^- ligand, which makes the formation of the neutral complex preferred, aiding in the isolation of the 3^M structural analogues for all the metal ions studied here.

A useful comparison can be made between the 2^M and 3^M series given their many similarities; however, one should bear

in mind the caveat that structural metrics between 2^M and 3^M may be affected by the differences in crystal packing systems, differences in the coordinating and non-coordinating solvents in the solid-state, as well as the presence of the contacting potassium ion in all of 2^M , which is absent in 3^M . Despite these differences, the coordination number and overall geometry about the metal centres in 3^M is comparable to that of 2^M , however, the coordinated THF molecule replaces the apical chloride ligand of the 2^M series commensurate with charge balance differences between the ‘-ate’ 2^M and neutral 3^M . For the 3^M series, all the M–[L^{Ar}] contact distances are like those in 2^M , with only a subtle contraction in bond distances observed. With regards to the M–C_{cent} values, going from 2^{Ce} to 3^{Ce} we see a decrease in the distance ($\Delta Ce-C_{cent} = -0.018 \text{ \AA}$) similar to that seen going from 2^{Np} to 3^{Np} ($\Delta Np-C_{cent} = -0.018 \text{ \AA}$), while going from 2^U to 3^U sees a modest increase in the distance ($\Delta U-C_{cent} = +0.007 \text{ \AA}$). Importantly, the M–C_{cent} trend seen in 2^M complexes, where the trend of M–arene distances deviates from that predicted by ionic radius, is mirrored in the 3^M series, but with the comparison now extending to include a Pu³⁺ complex.

As with the 2^M series, the uranium complex 3^U has the shortest M–arene bond distances of the 3^M series (Table 2). For instance, the U–C_{cent} value (2.538 (1) \AA) in 3^U is 0.108 \AA shorter than the Ce–C_{cent} in 3^{Ce} , slightly less than the magnitude of the M–C_{cent} difference between 2^U and 2^{Ce} of 0.134 \AA . This is due to the contraction of the Ce–C_{cent} distance from 3^{Ce} (2.646 (1) \AA) compared to 2^{Ce} (2.664 (1) \AA). Moreover, the U–C_{cent} value in 3^U is 0.023 \AA shorter than the Np–C_{cent} value in 3^{Np} , narrowing the difference of 0.049 \AA between 2^U and 2^{Np} . The Np–C_{cent} value in 3^{Np} is 0.086 \AA shorter than the Ce–C_{cent} value in 3^{Ce} . This tracks closely to a difference of 0.085 \AA between 2^{Np} and 2^{Ce} . Finally, consideration of the 3^{Pu} metrics shows that the value Pu–C_{cent} is 0.073 \AA shorter than the Ce–C_{cent} value in 3^{Ce} , 0.036 \AA longer than U–C_{cent} value in 3^U , and 0.013 \AA longer than the Np–C_{cent} value in 3^{Np} .

All told, there are two patterns which emerge across the M–C_{cent} distances in 2^M and 3^M : (a) all of the actinide arene centroid interactions are shorter than the corresponding cerium interactions despite similarities in ionic radii, and (b) the actinide arene–centroid distance appears to increase from U to Np to Pu, counter to the trend expected based on ionic radii alone, albeit with the acknowledgement that only the 3^M series can compare across all three actinide elements studied here (U, Np, Pu). Additionally, this trend is chiefly observed for the M–C_{arene} interaction and not consistently with any of the other M–ligand contacts. To visualize this trend with respect to the M–

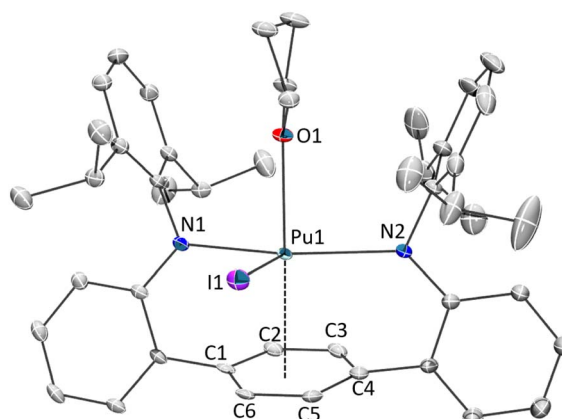


Fig. 3 ORTEP rendering of the solid-state molecular structures of $3^{Pu} \cdot THF_{0.66}Et_2O_{0.33}$. Hydrogen atoms and co-crystallized solvents are removed for clarity. Ellipsoids are shown at the 50% probability level. Complexes 3^{Ce} , 3^U and 3^{Np} are structurally analogous and can be found in the ESI for this document (S5–S7†).

Table 2 Selected bond metrics for the 3^M . Fractional solvents are indicated for those structures which contain substitutionally disordered lattice solvents

Complex	M–N bond distances (\AA) (N ₁ /N ₂)	M–cent distance (\AA)	M–C _{arene} range (\AA)	M–I distance (\AA)	N–M–N bond angle (°)	Metal ionic radius (\AA)
$3^{Ce} \cdot Et_2O$	2.509 (1)/2.441 (1)	2.646 (1)	2.943 (2)–3.047 (2) avg. 2.99	3.0810 (5)	156.32 (6)	1.01
$3^U \cdot THF_{0.8}Et_2O_{0.2}$	2.440 (1)/2.489 (1)	2.538 (1)	2.876 (1)–2.935 (1) avg. 2.90	3.0534 (7)	154.01 (5)	1.025
$3^{Np} \cdot Pent$	2.489 (8)/2.457 (7)	2.561 (4)	2.878 (8)–2.962 (9) avg. 2.91	3.0288 (9)	153.7 (3)	1.01
$3^{Pu} \cdot THF_{0.66}Et_2O_{0.33}$	2.469 (4)/2.428 (4)	2.574 (1)	2.902 (4)–2.970 (5) avg. 2.93	3.0276 (7)	153.97 (14)	1.00



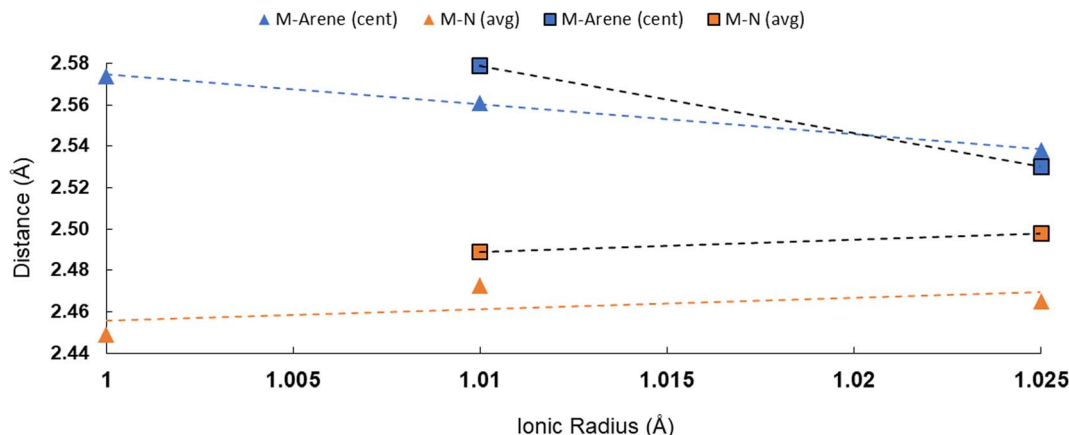


Fig. 4 Plot of metal ionic radius versus $M\text{-ligand}$ (N_{amide} and C_{cent}) bond distances for 2^M and 3^M complexes. Dotted lines shown were generated by linear trend line fits. Ionic radii values are for 6-coordinate An^{3+} species.⁶⁵

N_{amide} versus $M\text{-}C_{\text{cent}}$ distances, we have compiled them into graphical form in Fig. 4. For additional context, we have also compared the $M\text{-halide}$ distances and $M\text{-arene}$ distances for other molecular actinide series, which span relevant atoms of the 5f block (Fig. S39 and S40†). This break in observed bonding distances with predicted ionic radii/electrostatic interactions for the actinides is known, especially in respect to enhanced covalency in An^{3+} vs. Ln^{3+} systems, but we are not aware of documented instances of increasing metal-ligand bond length from U^{3+} to Np^{3+} to Pu^{3+} ,^{18,71–77} and such trends have not been examined for neutral arene interactions across those metals. The trend we observe here could be a result of covalency or steric effects, or both.

Turning to discussion of the 2^M and 3^M structures in the broader context of previously reported literature, the most noteworthy feature of these complexes is the metal-arene η^6 -interactions present. Examples of f-element interactions with formally neutral arenes for these metal ions are reported, with a handful of structurally verified reports for uranium,^{30,36,41,42,46,47,51–53,55,56,78–81} six for cerium,^{82–87} one for neptunium²¹ and none for plutonium at the time of writing. It should be noted that this type of interaction is also known for several rare-earth and lanthanide compounds, though here we focus on comparisons to similar f-element complexes (Ce, U, Np).

With respect to comparison against other uranium complexes, 2^U contains an average $U\text{-}C_{\text{arene}}$ bond distance of 2.89 Å and a $U\text{-}C_{\text{cent}}$ value of 2.538 (1) Å, which is in close agreement with 3^U which displays an average $U\text{-}C_{\text{arene}}$ bond distance of 2.90 Å and a $U\text{-}C_{\text{cent}}$ of 2.5384 (7) Å. These values are slightly shorter than our previously reported $L^{\text{Ar}}U^{\text{III}}(\text{I})(\text{DME})$ complex (avg. $U\text{-}C_{\text{arene}}$ = 2.92 Å, $U\text{-}C_{\text{cent}}$ = 2.56 Å).⁴⁶ Compared to other U^{3+} tethered-arene systems, the bis(arene) sandwich complex $\text{IU}(\text{NHAr}^{\text{Pr}})^2$, displays average $U\text{-}C_{\text{cent}}$ values 2.78 and 2.79 Å,⁴² while the bidentate $\text{LU}^{\text{III}}(\text{I})$ (L = *trans*-calix[2]benzene[2]pyrrolide) contains a $U\text{-}C_{\text{cent}}$ = 2.67 Å.⁴³ Although 2^U displays shorter $U\text{-}C_{\text{cent}}$ distances than the bis(arene) complexes noted above, the mono-arene U^{3+} complex, $\kappa^3\text{:}\eta^6\text{-}[(^{\text{Ad,Me}}\text{ArO})_3\text{mes}]U$

has significantly shorter average $U\text{-}C_{\text{arene}}$ distances of = 2.75 Å and $U\text{-}C_{\text{cent}}$ of 2.35 Å.⁴¹

Complexes 2^{Ce} and 3^{Ce} contain $M\text{-}C_{\text{arene}}$ interactions with average metal-arene contact distances of $\text{Ce-C}_{\text{arene}} = 3.01$ and 2.99 Å, respectively, with $\text{Ce-C}_{\text{cent}} = 2.664$ (1) and 2.646 (1) Å. These Ce^{3+} η^6 -arene interactions are intermediate compared to the unsupported terminal arene interactions of $\text{Ce}(\text{mes})\{N(\text{C}_6\text{F}_5)_2\}_3$ (avg. $\text{Ce-C}_{\text{arene}} = 3.15$ Å, $\text{Ce-C}_{\text{cent}} = 2.82$ Å),⁸⁴ and $\text{Ce}(\text{C}_6\text{H}_5\text{Me})(\text{GaCl}_4)_3$ (avg. $\text{Ce-C}_{\text{arene}} = 2.950$ Å, $\text{Ce-C}_{\text{cent}} = 2.61$ Å).⁸² Compared to the Ce^{2+} quadruple decker complex, $[\text{K}(2.2.2\text{-crypt})]_2[(\text{KL}_3\text{Ce})(\mu\text{-}\eta^6\text{-}\eta^6\text{-C}_7\text{H}_8)_2\text{Ce}]$, in which the Ce^{2+} centres are bridged by anionic toluene moieties supported by δ -bonding interactions, the $\text{Ce-C}_{\text{arene}}$ interactions are significantly shorter (avg. $\text{Ce1-C}_{\text{arene}} = 2.69$ Å and $\text{Ce2-C}_{\text{arene}} = 2.64$ Å) than in the case of 2^{Ce} and 3^{Ce} .⁸³

Complexes 1^{Np} , 2^{Np} and 3^{Np} represent rare examples of formally neutral η^6 -arenes bound to neptunium. To our knowledge, only one such other example is reported in the literature consisting of the complexes $\text{LNp}^{\text{III}}(\text{Cl})$ and $[(\text{L})\text{Np}^{\text{III}}_2\text{Cl}_4(\text{THF})_3]$ where (L = *trans*-calix[2]benzene[2]pyrrolide).²¹ In this reported case, the Np -arene interactions were suggested to be key constituents which allow for the formation of an intermediate putative Np^{2+} complex, as supported by spectroscopic data. The Np η^6 -arene interactions in 2^{Np} and 3^{Np} ($\text{Np-C}_{\text{cent}} = 2.579$ (2) and 2.561 (4) Å, respectively) are slightly shorter than those of $\text{LNp}^{\text{III}}(\text{Cl})$ ($\text{Np-C}_{\text{cent}} = 2.60$ Å) and $[(\text{L})\text{Np}^{\text{III}}_2\text{Cl}_4(\text{THF})_3]$ ($\text{Np-C}_{\text{cent}} = 2.63$ Å).

UV-vis-NIR spectra were measured on solutions (THF or toluene) of 1^M , 2^M and 3^M . All complexes share broad absorption features in the UV-vis region (Fig. S17–S25†) that extend out to 500–700 nm and are characteristic of charge transfer (CT) activity, and is consistent with those reported for other complexes of the $[L^{\text{Ar}}]$ ligand platform.^{46,47,60} It is important to note, as mentioned earlier, the presence of small amounts of $\text{H}_2\text{L}^{\text{Ar}}$ impurities may have minor contributions to the absorption bands in the UV-vis region of these spectra. The near-IR (NIR) absorption features of 2^U and 3^U (Fig. 5a) are comparable with minor shifts in peak location and are quite similar to



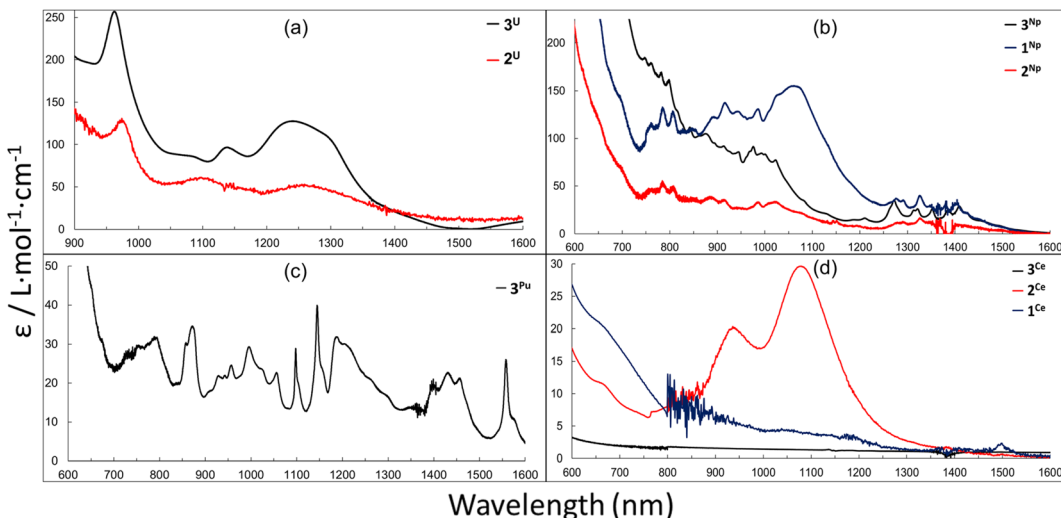


Fig. 5 (a): NIR spectra for 2^U (4.6 mM in Tol) and 3^U (3.0 mM in THF). (b): vis-NIR spectra for the 1^{Np} , 2^{Np} and 3^{Np} series. (0.69 mM in Tol, 0.50 mM in Tol and 2.1 mM in THF respectively). (c): vis-NIR spectra for 3^{Pu} (1.0 mM in THF). (d): vis-NIR spectra of 3^{Ce} , 2^{Ce} and 1^{Ce} (9.51 mM, 5.86 mM and 2.32 mM respectively) in toluene.

the U^{3+} complex, $L^{Ar}U(i)(DME)$, where the bands are consistent with 5f-5f transitions for U^{3+} .⁴⁶

Complexes 1^{Np} , 2^{Np} and 3^{Np} display a series of weak absorptions observed in the NIR region from 700–1355 nm, consistent with Laporte-forbidden 5f-5f transitions and typical of many neptunium complexes in the trivalent oxidation state.^{75,88,89} The three spectra are qualitatively similar, although the broad feature centred around 1069 nm present in 1^{Np} is largely absent in the spectra of 2^{Np} and 3^{Np} (Fig. 5b). The more intense nature of the bands in all three Np spectra in the ~700–1100 nm region may also be consistent with 5f-6d transitions and/or 5f-6d/5f/5f transitions.

Complex 3^{Pu} contains a number of broad and sharp features with low absorption coefficients ($\epsilon/L\text{ mol}^{-1}\text{ cm}^{-1} > 50$) between 550–1600 nm (Fig. 5c), which is consistent with 5f-5f transitions often observed for other Pu^{3+} complexes.^{69,75,90,91} The absence of more intense transitions in the ~700–1100 nm region (in contrast to the Np spectra) could be because the increasing 5f-6d energy gap as the actinide series is traversed means that those transitions shift to higher energy and are either mixed with the charge-transfer region or outside the spectral window. Interestingly, 2^{Ce} displays two weak, broad features in the NIR region centred at 937 and 1080 nm, while the spectra of the neutral complexes 1^{Ce} and 3^{Ce} are silent in the NIR region (Fig. 5d). We have yet to attribute these features and it is possible that they arise from impurities from synthesis or instability in solution.

Conclusions

Through the use of terphenyl bis(anilide) ligand $[(K(DME)_2)_2 \cdot L^{Ar}]$, ($L^{Ar} = \{C_6H_4[(2,6-iPr^2C_6H_3)NC_6H_4]_2\}^{2-}$), we installed tethered η^6 -arene interactions onto various trivalent 4f and 5f-block ions to isolate complex types 1^M , 2^M and 3^M . These series include the formation of rare, neptunium η^6 -arene complexes 1^{Np} , 2^{Np} and 3^{Np} as well as a first structurally documented

plutonium η^6 -arene interaction in 3^{Pu} . Taken together, the structural analysis and the UV-vis-NIR studies are consistent with the M^{3+} assignments for the metal oxidation state in the complexes with the coordinated η^6 -arene possessing neutral character.

Of particular note, structural analyses of the reported complexes show a preference for shorter $M-C_{\text{arene}}$ bonds for the U^{3+} complex over the Np^{3+} , Pu^{3+} and Ce^{3+} complexes, despite U^{3+} having the larger reported ionic radius. Notwithstanding the longer $M-C_{\text{arene}}$ bonds for the Np^{3+} and Pu^{3+} complexes relative to U^{3+} , both are still notably shorter than in the Ce^{3+} congeners. These bond metrics fail to adhere to structural trends predicted by a purely electrostatic model. This possibly indicates enhanced metal-arene orbital overlap in the case of the actinide ions as compared to cerium, which would be expected due to the greater ability of these elements to participate in covalent bonding interactions over their 4f-counterparts. Furthermore, this structural data points to an interesting phenomenon in these complexes that the $U-C_{\text{arene}}$ bonds trend shorter than the $Np-C_{\text{arene}}$ and $Pu-C_{\text{arene}}$ bonds, counter to almost all other homologous series of U, Np and Pu complexes which exhibit shortening of the actinide ligands bond lengths from uranium across to plutonium within the trivalent oxidation state.

Complexes 1^M , 2^M and 3^M represent an underexplored area of f-block chemical research, in which closely related complexes spanning the lanthanides and actinides can be evaluated for structural and electronic trends. Especially pertinent is the presence of the η^6 -arene interactions, which serve as an unusual model to probe the nature of bonding among the f-block and expose any underlying periodicity. We anticipate potential for further reactivity studies on the reported complexes, including redox examinations to assess the ability for these complexes to support high and low-valent metal species, along with electronic structure analysis.



Author contributions

J. M. led and performed lanthanide and actinide synthetic experimental work, compound characterization data collection, and was principally responsible for manuscript drafting. C. A. P. G. and L. S. assisted with transuranium experimental work. S. F. and A. J. G. were the project principal investigators. S. F. conceptualized the synthesis of reported compounds and assisted in experimental work. A. J. G. supervised development of transuranium synthetic strategies and experimental work. B. L. S. supervised the single crystal X-ray data collection and assisted in structure refinements. All authors contributed to the manuscript writing, editing, and review process.

Conflicts of interest

There are no conflicts to declare.

Acknowledgements

Transuranium work was conducted at Los Alamos National Laboratory (LANL) for which A. J. G., J. M. and B. L. S. acknowledge the U.S. Department of Energy, Office of Science, Office of Basic Energy Sciences, Chemical Sciences, Geosciences, and Biosciences Division, Heavy Element Chemistry Program at LANL (DE-AC52-06NA25396). J. M. also thanks the LANL G. T. Seaborg Institute for Graduate Summer Student and Postdoctoral Fellowships, provided the Laboratory Directed Research and Development (LDRD) programs. C. A. P. G. was supported by a J. R. Oppenheimer Distinguished Postdoctoral Fellowship under LANL-LDRD funding (20180703PRD1). S. F. is grateful to the Welch Foundation (AH-1922-20200401) and the UTEP NSF-PREM program (DMR-1827745) for financial support of this work. Partial crystallographic support was made possible through the NSF-MRI program (S. F.; CHE-1827875).

Notes and references

- 1 G. T. Seaborg, in *Handbook on the Physics and Chemistry of Rare Earths*, Elsevier, 1994, vol. 18, pp. 1–27.
- 2 D. Freedman, J. H. Melman, T. J. Emge and J. G. Brennan, *Inorg. Chem.*, 1998, **37**, 4162–4163.
- 3 J. L. Krinsky, S. G. Minasian and J. Arnold, *Inorg. Chem.*, 2011, **50**, 345–357.
- 4 C. J. Burns and B. E. Bursten, *Comments Inorg. Chem.*, 1989, **9**, 61–93.
- 5 D. L. Clark, J. C. Gordon, P. J. Hay and R. Poli, *Organometallics*, 2005, **24**, 5747–5758.
- 6 G. R. Choppin, *J. Alloys Compd.*, 2002, **344**, 55–59.
- 7 T. W. Hayton, *Dalton Trans.*, 2010, **39**, 1145–1158.
- 8 M. L. Neidig, D. L. Clark and R. L. Martin, *Coord. Chem. Rev.*, 2013, **257**, 394–406.
- 9 A. Formanuik, A.-M. Ariciu, F. Ortu, R. Beekmeyer, A. Kerridge, F. Tuna, E. J. L. McInnes and D. P. Mills, *Nat. Chem.*, 2017, **9**, 578–583.
- 10 M. W. Löble, J. M. Keith, A. B. Altman, S. C. E. Stieber, E. R. Batista, K. S. Boland, S. D. Conradson, D. L. Clark, J. Lezama Pacheco, S. A. Kozimor, R. L. Martin, S. G. Minasian, A. C. Olson, B. L. Scott, D. K. Shuh, T. Tyliszczak, M. P. Wilkerson and R. A. Zehnder, *J. Am. Chem. Soc.*, 2015, **137**, 2506–2523.
- 11 N. L. Eatough and H. T. Hall, *Inorg. Chem.*, 1970, **9**, 417–418.
- 12 S. A. Kozimor, P. Yang, E. R. Batista, K. S. Boland, C. J. Burns, D. L. Clark, S. D. Conradson, R. L. Martin, M. P. Wilkerson and L. E. Wolfsberg, *J. Am. Chem. Soc.*, 2009, **131**, 12125–12136.
- 13 S. G. Minasian, J. M. Keith, E. R. Batista, K. S. Boland, D. L. Clark, S. D. Conradson, S. A. Kozimor, R. L. Martin, D. E. Schwarz, D. K. Shuh, G. L. Wagner, M. P. Wilkerson, L. E. Wolfsberg and P. Yang, *J. Am. Chem. Soc.*, 2012, **134**, 5586–5597.
- 14 R. M. Diamond, K. Street and G. T. Seaborg, *J. Am. Chem. Soc.*, 1954, **76**, 1461–1469.
- 15 E. Lu, S. Sajjad, V. E. J. Berryman, A. J. Woole, N. Kaltsoyannis and S. T. Liddle, *Nat. Commun.*, 2019, **10**, 634.
- 16 T. Vitova, I. Pidchenko, D. Fellhauer, P. S. Bagus, Y. Joly, T. Pruessmann, S. Bahl, E. Gonzalez-Robles, J. Rothe, M. Altmaier, M. A. Denecke and H. Geckeis, *Nat. Commun.*, 2017, **8**, 16053.
- 17 A. Kerridge, *Chem. Commun.*, 2017, **53**, 6685–6695.
- 18 A. J. Gaunt, S. D. Reilly, A. E. Enriquez, B. L. Scott, J. A. Ibers, P. Sekar, K. I. M. Ingram, N. Kaltsoyannis and M. P. Neu, *Inorg. Chem.*, 2008, **47**, 29–41.
- 19 J. T. Brewster II, D. N. Mangel, A. J. Gaunt, D. P. Saunders, H. Zafar, V. M. Lynch, M. A. Boreen, M. E. Garner, C. A. P. Goodwin, N. S. Settineri, J. Arnold and J. L. Sessler, *J. Am. Chem. Soc.*, 2019, **141**, 17867–17874.
- 20 J. Su, T. Cheisson, A. McSkimming, C. A. P. Goodwin, I. M. DiMucci, T. Albrecht-Schönzart, B. L. Scott, E. R. Batista, A. J. Gaunt, S. A. Kozimor, P. Yang and E. J. Schelter, *Chem. Sci.*, 2021, **12**, 13343–13359.
- 21 M. S. Dutkiewicz, J. H. Farnaby, C. Apostolidis, E. Colineau, O. Walter, N. Magnani, M. G. Gardiner, J. B. Love, N. Kaltsoyannis, R. Caciuffo and P. L. Arnold, *Nat. Chem.*, 2016, **8**, 797–802.
- 22 J. J. Shephard, V. E. J. Berryman, T. Ochiai, O. Walter, A. N. Price, M. R. Warren, P. L. Arnold, N. Kaltsoyannis and S. Parsons, *Nat. Commun.*, 2022, **13**, 5923.
- 23 M. S. Dutkiewicz, C. A. P. Goodwin, M. Perfetti, A. J. Gaunt, J.-C. Griveau, E. Colineau, A. Kovács, A. J. Woole, R. Caciuffo, O. Walter and S. T. Liddle, *Nat. Chem.*, 2022, **14**, 342–349.
- 24 W. A. King, T. J. Marks, D. M. Anderson, D. J. Duncalf and F. G. N. Cloke, *J. Am. Chem. Soc.*, 1992, **114**, 9221–9223.
- 25 M. N. Bochkarev, *Chem. Rev.*, 2002, **102**, 2089–2118.
- 26 O. Walter, *Chem.-Eur. J.*, 2019, **25**, 2927–2934.
- 27 N. Kaltsoyannis, *Chem.-Eur. J.*, 2018, **24**, 2815–2825.
- 28 J. Murillo, R. Bhowmick, K. L. M. Harriman, A. Gomez-Torres, J. Wright, R. W. Meulenbergh, P. Miró, A. Metta-Magaña, M. Murugesu, B. Vlaisavljevich and S. Fortier, *Chem. Sci.*, 2021, **12**, 13360–13372.
- 29 J. Murillo, R. Bhowmick, K. L. M. Harriman, A. Gomez-Torres, J. Wright, P. Miró, A. Metta-Magaña, M. Murugesu,



B. Vlaisavljevich and S. Fortier, *Chem. Commun.*, 2022, **58**, 9112–9115.

30 F. Y. T. Lam, J. A. L. Wells, T. Ochiai, C. J. V. Halliday, K. N. McCabe, L. Maron and P. L. Arnold, *Inorg. Chem.*, 2022, **61**, 4581–4591.

31 P. L. Diaconescu, P. L. Arnold, T. A. Baker, D. J. Mindiola and C. C. Cummins, *J. Am. Chem. Soc.*, 2000, **122**, 6108–6109.

32 W. J. Evans, S. A. Kozimor, J. W. Ziller and N. Kaltsoyannis, *J. Am. Chem. Soc.*, 2004, **126**, 14533–14547.

33 M. P. Kelley, I. A. Popov, J. Jung, E. R. Batista and P. Yang, *Nat. Commun.*, 2020, **11**, 1558.

34 S. G. Minasian, J. M. Keith, E. R. Batista, K. S. Boland, D. L. Clark, S. A. Kozimor, R. L. Martin, D. K. Shuh and T. Tyliszczak, *Chem. Sci.*, 2014, **5**, 351–359.

35 H. S. La Pierre, A. Scheurer, F. W. Heinemann, W. Hieringer and K. Meyer, *Angew. Chem., Int. Ed.*, 2014, **53**, 7158–7162.

36 S. M. Franke, B. L. Tran, F. W. Heinemann, W. Hieringer, D. J. Mindiola and K. Meyer, *Inorg. Chem.*, 2013, **52**, 10552–10558.

37 I. A. Popov, B. S. Billow, S. H. Carpenter, E. R. Batista, J. M. Boncella, A. M. Tondreau and P. Yang, *Chem.-Eur. J.*, 2022, **28**, e202200114.

38 D. Seyferth, *Organometallics*, 2002, **21**, 2800–2820.

39 S. C. Bart, F. W. Heinemann, C. Anthon, C. Hauser and K. Meyer, *Inorg. Chem.*, 2009, **48**, 9419–9426.

40 D. P. Halter, H. S. La Pierre, F. W. Heinemann and K. Meyer, *Inorg. Chem.*, 2014, **53**, 8418–8424.

41 H. S. La Pierre, H. Kameo, D. P. Halter, F. W. Heinemann and K. Meyer, *Angew. Chem., Int. Ed.*, 2014, **53**, 7154–7157.

42 B. S. Billow, B. N. Livesay, C. C. Mokhtarzadeh, J. McCracken, M. P. Shores, J. M. Boncella and A. L. Odom, *J. Am. Chem. Soc.*, 2018, **140**, 17369–17373.

43 P. L. Arnold, J. H. Farnaby, R. C. White, N. Kaltsoyannis, M. G. Gardiner and J. B. Love, *Chem. Sci.*, 2014, **5**, 756–765.

44 P. L. Arnold, J. H. Farnaby, M. G. Gardiner and J. B. Love, *Organometallics*, 2015, **34**, 2114–2117.

45 M. Suvova, K. T. P. O'Brien, J. H. Farnaby, J. B. Love, N. Kaltsoyannis and P. L. Arnold, *Organometallics*, 2017, **36**, 4669–4681.

46 S. Fortier, J. R. Aguilar-Calderon, B. Vlaisavljevich, A. J. Metta-Magaña, A. G. Goos and C. E. Botez, *Organometallics*, 2017, **36**, 4591–4599.

47 M. Yadav, A. J. Metta-Magaña and S. Fortier, *Chem. Sci.*, 2020, **11**, 2381–2387.

48 C. J. Inman, A. S. P. Frey, A. F. R. Kilpatrick, F. G. N. Cloke and S. M. Roe, *Organometallics*, 2017, **36**, 4539–4545.

49 M. D. Straub, E. T. Ouellette, M. A. Boreen, R. D. Britt, K. Chakarawet, I. Douair, C. A. Gould, L. Maron, I. Del Rosal, D. Villarreal, S. G. Minasian and J. Arnold, *J. Am. Chem. Soc.*, 2021, **143**, 19748–19760.

50 J. Murillo and S. Fortier, in *Encyclopedia of Inorganic and Bioinorganic Chemistry*, 2018, pp. 1–19.

51 M. Cesari, U. Pedretti, Z. Zazzetta, G. Lugli and W. Marconi, *Inorg. Chim. Acta*, 1971, **5**, 439–444.

52 F. A. Cotton and W. Schwotzer, *Organometallics*, 1985, **4**, 942–943.

53 F. A. Cotton and W. Schwotzer, *Organometallics*, 1987, **6**, 1275–1280.

54 G. C. Campbell, F. A. Cotton, J. F. Haw and W. Schwotzer, *Organometallics*, 1986, **5**, 274–279.

55 F. A. Cotton, W. Schwotzer and C. Q. Simpson II, *Angew. Chem., Int. Ed. Engl.*, 1986, **25**, 637–639.

56 D. Baudry, E. Bulot, P. Charpin, M. Ephritikhine, M. Lance, M. Nierlich and J. Vigner, *J. Organomet. Chem.*, 1989, **371**, 155–162.

57 V. Paprocki, P. Hrobárik, K. L. M. Harriman, M. S. Luff, T. Kupfer, M. Kaupp, M. Murugesu and H. Braunschweig, *Angew. Chem., Int. Ed.*, 2020, **59**, 13109–13115.

58 D. P. Halter, F. W. Heinemann, L. Maron and K. Meyer, *Nat. Chem.*, 2018, **10**, 259–267.

59 D. P. Halter, F. W. Heinemann, J. Bachmann and K. Meyer, *Nature*, 2016, **530**, 317–321.

60 K. L. M. Harriman, J. Murillo, E. A. Suturina, S. Fortier and M. Murugesu, *Inorg. Chem. Front.*, 2020, **7**, 4805–4812.

61 S. D. Daniel, J.-S. M. Lehn, J. D. Korp and D. M. Hoffman, *Polyhedron*, 2006, **25**, 205–210.

62 X. Xin and C. Zhu, *Dalton Trans.*, 2020, **49**, 603–607.

63 E. M. Broderick, P. S. Thuy-Boun, N. Guo, C. S. Vogel, J. Sutter, J. T. Miller, K. Meyer and P. L. Diaconescu, *Inorg. Chem.*, 2011, **50**, 2870–2877.

64 S. M. Mansell, B. F. Perandones and P. L. Arnold, *J. Organomet. Chem.*, 2010, **695**, 2814–2821.

65 R. D. Shannon, *Acta Crystallogr., Sect. A*, 1976, **32**, 751–767.

66 S. G. Kukolich, *J. Am. Chem. Soc.*, 1995, **117**, 5512–5514.

67 S. M. Hubig, S. V. Lindeman and J. K. Kochi, *Coord. Chem. Rev.*, 2000, **200**–202, 831–873.

68 P. Le Maguères, S. V. Lindeman and J. K. Kochi, *Organometallics*, 2001, **20**, 115–125.

69 C. A. P. Goodwin, M. T. Janicke, B. L. Scott and A. J. Gaunt, *J. Am. Chem. Soc.*, 2021, **143**, 20680–20696.

70 K. Izod, S. T. Liddle and W. Clegg, *Inorg. Chem.*, 2004, **43**, 214–218.

71 J. Su, E. R. Batista, K. S. Boland, S. E. Bone, J. A. Bradley, S. K. Cary, D. L. Clark, S. D. Conradson, A. S. Ditter, N. Kaltsoyannis, J. M. Keith, A. Kerridge, S. A. Kozimor, M. W. Löble, R. L. Martin, S. G. Minasian, V. Mocko, H. S. La Pierre, G. T. Seidler, D. K. Shuh, M. P. Wilkerson, L. E. Wolfsberg and P. Yang, *J. Am. Chem. Soc.*, 2018, **140**, 17977–17984.

72 C. Tamain, M. Autillo, D. Guillaumont, L. Guérin, R. E. Wilson and C. Berthon, *Inorg. Chem.*, 2022, **61**, 12337–12348.

73 M. Autillo, R. E. Wilson, M. Vasiliu, G. F. de Melo and D. A. Dixon, *Inorg. Chem.*, 2022, **61**, 15607–15618.

74 T. Radoske, J. März, M. Patzschke, P. Kaden, O. Walter, M. Schmidt and T. Stumpf, *Chem. – Eur. J.*, 2020, **26**, 16853–16859.

75 C. A. P. Goodwin, S. R. Ciccone, S. Bekoe, S. Majumdar, B. L. Scott, J. W. Ziller, A. J. Gaunt, F. Furche and W. J. Evans, *Chem. Commun.*, 2022, **58**, 997–1000.

76 R. Kloditz, S. Fichter, S. Kaufmann, T. S. Brunner, P. Kaden, M. Patzschke, T. Stumpf, P. W. Roesky, M. Schmidt and J. März, *Inorg. Chem.*, 2020, **59**, 15670–15680.



77 D. D. Schnaars, A. J. Gaunt, T. W. Hayton, M. B. Jones, I. Kirker, N. Kaltsoyannis, I. May, S. D. Reilly, B. L. Scott and G. Wu, *Inorg. Chem.*, 2012, **51**, 8557–8566.

78 D. Pividori, M. E. Miehlich, B. Kestel, F. W. Heinemann, A. Scheurer, M. Patzschke and K. Meyer, *Inorg. Chem.*, 2021, **60**, 16455–16465.

79 W. G. Van der Sluys, C. J. Burns, J. C. Huffman and A. P. Sattelberger, *J. Am. Chem. Soc.*, 1988, **110**, 5924–5925.

80 W. J. Evans, S. A. Kozimor, W. R. Hillman and J. W. Ziller, *Organometallics*, 2005, **24**, 4676–4683.

81 P. L. Arnold, C. J. Stevens, J. H. Farnaby, M. G. Gardiner, G. S. Nichol and J. B. Love, *J. Am. Chem. Soc.*, 2014, **136**, 10218–10221.

82 M. Gorlov, L. L. Hussami, A. Fischer and L. Kloo, *Eur. J. Inorg. Chem.*, 2008, **2008**, 5191–5195.

83 R. P. Kelly, L. Maron, R. Scopelliti and M. Mazzanti, *Angew. Chem., Int. Ed.*, 2017, **56**, 15663–15666.

84 H. Yin, A. J. Lewis, P. Carroll and E. J. Schelter, *Inorg. Chem.*, 2013, **52**, 8234–8243.

85 G. B. Deacon, T. Feng, C. M. Forsyth, A. Gitlits, D. C. R. Hockless, Q. Shen, B. W. Skelton and A. H. White, *J. Chem. Soc., Dalton Trans.*, 2000, 961–966.

86 A. N. Selikhov, A. V. Cherkasov, K. A. Lyssenko and A. A. Trifonov, *Organometallics*, 2022, **41**, 820–828.

87 M. E. Hossain, Z. Guo, J. Wang, G. B. Deacon, P. C. Junk, D. Diether and R. Anwander, *Eur. J. Inorg. Chem.*, 2022, **2022**, e202101009.

88 S. A. Pattenaud, N. H. Anderson, S. C. Bart, A. J. Gaunt and B. L. Scott, *Chem. Commun.*, 2018, **54**, 6113–6116.

89 A. J. Myers, M. L. Tarlton, S. P. Kelley, W. W. Lukens and J. R. Walensky, *Angew. Chem., Int. Ed.*, 2019, **58**, 14891–14895.

90 C. J. Windorff, J. M. Sperling, T. E. Albrecht-Schönzart, Z. Bai, W. J. Evans, A. N. Gaiser, A. J. Gaunt, C. A. P. Goodwin, D. E. Hobart, Z. K. Huffman, D. N. Huh, B. E. Klamm, T. N. Poe and E. Warzecha, *Inorg. Chem.*, 2020, **59**, 13301–13314.

91 L. R. Avens, S. G. Bott, D. L. Clark, A. P. Sattelberger, J. G. Watkin and B. D. Zwick, *Inorg. Chem.*, 1994, **33**, 2248–2256.

